18th International Conference
ENGINEERING MECHANICS 2012
Svratka, Czech Republic, May 14 – 17, 2012

pp. 825–834
Paper #177

EARLY DEFECT DETECTION OF ACETABULAR IMPLANTS

D. Kytýř, O. Jiroušek, P. Zlámal, T. Doktor [*], I. Jandejsek [**]

Abstract: *The paper is focused on possibilities of modern X-ray detectors and micro-focus X-ray source for investigation of early degradation processes of acetabular implants. To simulate the most adverse activity (downstairs walking) a hip joint simulator was developed. The experimental setup was designed for cyclic loading of polyethylene acetabular cup implanted into the human pelvic bone and fixed by commercial polymethyl methacrylate bone cement. To predict the bone degradation numerical analysis of detailed three-dimensional model of the acetabular cup and the cement mantle implanted in a bone block was performed. Using large area flat panel detector and microfocus X-ray source it is possible to investigate micro-damage propagation and detect early defect in the bone-implant interface.*

Keywords: ***bone–cement interface, computed tomography, crack detection, hip simulator***

1. Introduction

Total hip arthroplasty has emerged as one of the most successful interventions in orthopaedics. In spite of the successful use of the total endoprosthesis there is still a number of problems connected with the artificially created co-existence and interaction between the bone tissue and the technical substances of the endoprosthesis. From an engineering perspective these must be designed with the sufficient mechanical strength and be able to endure the biological environment in which they are placed. In order to reduce the incidence of an implant failure, it is important that the entire system is fully characterized; from the anatomy of the joint and the biological response, through to the micro-structure of the material and the design geometry.

Micro-motions and consecutive loosening of the acetabular implant is one of the most serious therapeutic complications which often occurs several years after the implantation. Worldwide experiences demonstrate that $80\,\%$ of all revised endoprosthesis are damaged by the aseptic loosening. The important part in the this process is remodelling of bone tissue as a result of the change of the stress field after the implantation. Living bone tissue is continuously in the process of growing, strengthening and resorption; a process called bone remodelling. Initial cancellous bone adapts its internal structure by trabecular surface remodelling to accomplish its mechanical function as a load bearing structure. In the case of cemented acetabular implants the remaining cartilage is removed from the acetabulum and the shape is adapted to the original one by means of a spherical milling machine. With this procedure a roughly spherical bed is obtained. The size and character of the contact stress distribution in subchondral bone influences the cement mantle degradation and the primary stability of the implant.

2. Materials and methods

To determine the degradation caused by cyclic mechanical loading radiological investigation have been used. Cement layer degradation were investigated using using hip simulator. To predict the bone degradation numerical analysis of detailed three-dimensional model of the acetabular cup and the cement mantle implanted in a bone block was performed. Image data from μCT were used to reconstruct the complex geometry of the inner structure of the trabecular bone and the interface between the pelvic bone and the implant. Visualization of trabecular bone structure and cement layer changes (damage accumulation) provided information about implant instability progress.

[*]Daniel Kytýř, Ondřej Jiroušek, Petr Zlámal, Tomáš Doktor: Institute of Theoretical and Applied Mechanics AS CR, v. v. i., Prosecká 76, 190 00 Prague 9, email: {kytyr, jirousek, zlamal, doktor}@itam.cas.cz
[**]Ivan Jandejsek: Czech Technical University in Prague, Institute of Experimental and Applied Physics, Horská 3a/22, 128 00 Praha 2 email: jandejs@itam.cas.cz

2.1. Hemipelvic bone specimen

The experiments and measurements were carried out using wet anatomical specimen of a hemipelvic bone from female donor. With regards to microtomography device detector size it was necessary to cut down the specimen to fit the detector. The bone was resected in ischial, pubic and iliac part; the acetabular area remained intact. Cemented acetabular cup with its rim made of ultra-high molecular weight polyethylene (UHMWPE) was implanted. For proper function of the cup and its fixation was essential that the layer of cement was equally strong across the interface between the surface of a polyethylene cup and machined acetabulum. Well compression into a bone bed and the grooves on the surface of the cup obviated case rotation and movement of the implant. The implantation procedure depicted on Fig.1 consists of four basic steps:

- After removal of large boundary osteophytes was acetabulum emended by rasper cutter at an angle of $45\,^{\circ}$ from the longitudinal axis of the patient
- Customized acetabulum was drilled to make a anchor slots for the bone cement
- The bone cement was formed into a shape of acetabular cup. The cap was placed and fixed. Horizontal declination of the cap from the frontal plane was $45\,^{\circ}$ The centration was facilitated by horizontal support arm of cap loader, which is parallel to the operating table and the longitudinal axis of the patient.
- Final location of the implant was checked using protractor on the vertical arm.

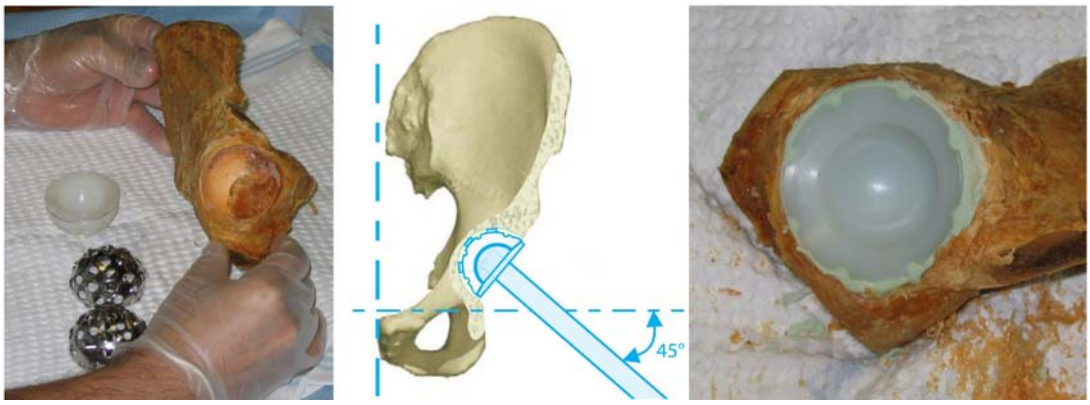

Fig. 1: Acetabular component implantation procedure

2.2. Bone specimen for material testing

Knowledge of material properties is a prerequisite to perform mechanical analysis, especially in case of numerical simulations. There is a very wide range of trabecular bone material properties ($E = 0.1 - 4.5\,\mathrm{GPa}$) reported in literature, see Dalstra (1993) and Hanson (2004), almost no correlation between the Young's modulus and anatomical location. To obtain mechanical properties of the trabecular bone time-resolved X-ray microtomography described in Jirousek & Zlamal (2011) and Digital Volume Correlation (DVC) presented by Jirousek & Jandejsek (2011) was employed.

Regard to the cancellous bone microstructure composed of trabeculae (approximately with length $1000\,\mu\mathrm{m}$ and thickness $150\,\mu\mathrm{m}$) the sapmle $12\,\mathrm{mm}$ high and $10\,\mathrm{mm}$ in diameter was drill out from proximal femur.

Special loading device was designed for this purpose. The frame of the device was made from plastic material with very low absorption of X-rays. The sample was fixed in an cylindrical chamber and loaded. The incremental loading with $100\,\mu\mathrm{m}$ increments up to $10\,\%$ deformation was applied in the experiment. The loading device was mounted on a rotational table and placed between the X-ray source and detector. Microfocus X-ray source L8601-01 (Hamamatsu Photonics K.K.)was used together with X-ray detector

Medipix-2, see Jakubek (2007), for the imaging. The detector chip is equipped with a single common backside electrode and a front side matrix of electrodes. The active area of the detector with $55\,\mu\mathrm{m}$ pitch provides images with resolution $256 \times 256\,\mathrm{px}$.

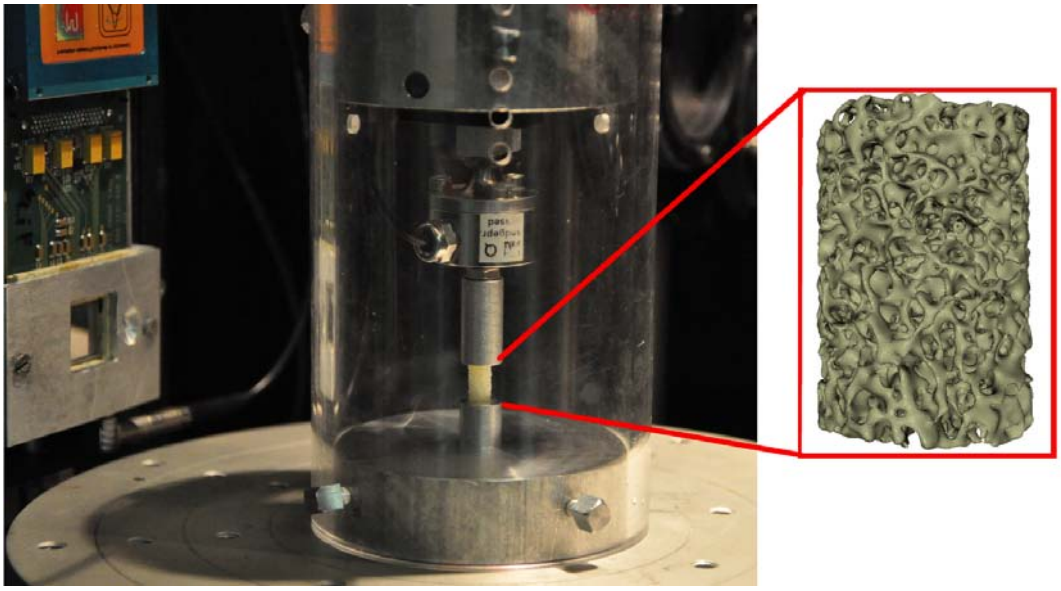

Fig. 2: Detail of loading device placed between X-ray source and detector with reconstructed specimen based on μCT data

DVC is a novel technique for 3D strain and deformation measurements across entire material volumes can be described in four steps: (i) control points in which the displacements will be tracked are defined in the image data, (ii) image correlation is performed in a $20 \times 20 \times 20\,\mathrm{px}$ image subvolume around the control point, (iii) displacement of each of the control points is computed by minimizing the 3D correlation coefficient by using nonlinear optimization techniques, (iv) the strains are computed from the established displacements and of the control points and overall mechanical properties ($E = 0.853\,\mathrm{GPa}$) are obtained.

2.3. Numerical analysis

To obtain a better information about stress distribution during the gait cycle (one step) and location of early defect regions the numerical simulation was performed. Finite element model of acetabular socket with cement layer and acetabular component was developed. The gait analysis (downstair gait cycle) consists of sequence of 20 loadsteps.

2.4. Model development

Based on implant manufacturer (Beznoska s.r.o.) datasheed detailed geometrical model was created. Four separately components was modeled. Femoral component was modeled as a spherical head with ($\oslash D = 32\,\mathrm{mm}$) and the cylindrical neck. Acetabular implant with inner diameter $32\,\mathrm{mm}$and outer diameter $49\,\mathrm{mm}$ was modeled with all construction detail without any simplification. The cement layer was created as a imprint of the implant and one surface and hemisphere at other side. The thickness of mantle was $3\,\mathrm{mm}$. This layer was surrounded by cylindrical socket bone socket.

10-node tetrahedral elements was chosen for meshing of all components because of the thin geometry and small radius of the cement mantle model. The simulation was assumed to be quasistatic, divided in 20 loadsteps. The loading force value and the direction of downstair walking in each load step was measured by Bergmann (2001). The contact was used for more accurate force transmission to the pelvis. The model was constrained by fixation of all degrees of freedom at the bottom part.

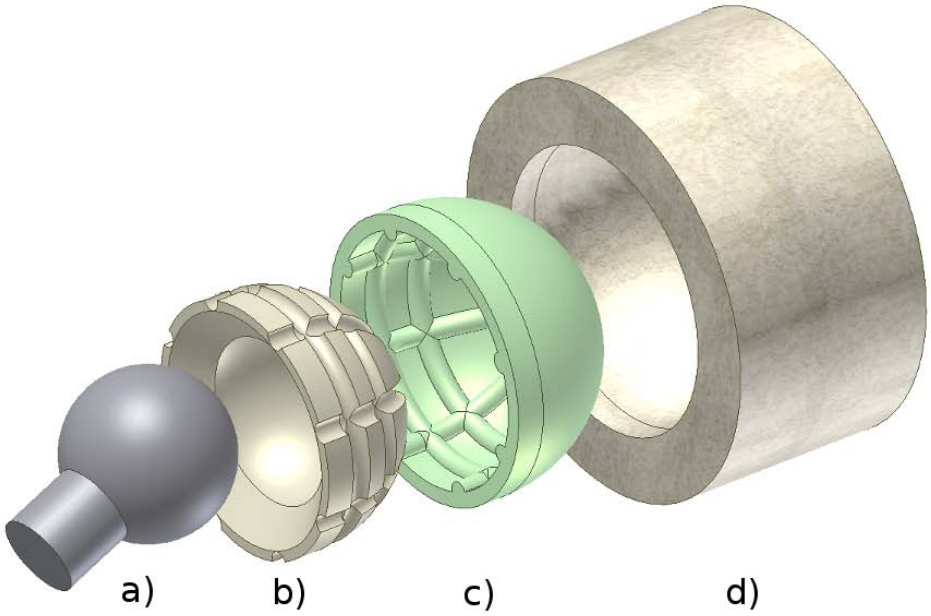

Fig. 3: Hip replacement CAD model composed of a) femoral component b) acetabular component c) cement layer d) bone socket

2.5. Contact definition

In accordance with Ansys modeling approaches, surface-to-surface contact was defined between head and acetabular component. Elastic modulus of steel femoral part was more than three hundred times higher than plastic cup; therefore the rigid-to-flexible method was used. The head and the inner hemisphere of the cup was meshed by special elements to model the femoro-acetabular interface. Both types of contact elements were second-order 8-nodes. For rigid-to-flexible contact designation the target surface is always the rigid surface and the contact surface is always the deformable surface. Contact elements are constrained against penetrating the target surface. However, target elements can penetrate through the contact surface. To ensure a proper function of the contact it is necessary that all contact and target element normals have opposite direction. Friction between the femoral head and the acetabular cup was neglected. For better numerical stability the femoral and acetabular component was connected by very flexible spar elements with no influence to stress distribution in pelvis.

2.6. Used materials

Material properties are described in Tab. 1. All materials were considered as isotropic linear elastic. Trabecular bone material properties were obtained by experimental measurement, the properties of the stainless steel, UHMWPE (ISO 5834 -2) and the bone-cement Palacos R (Heraeus Medical, GmbH) were provided by the manufacturers.

Tab. 1: Material properties

Material	Young's modulus [GPa]	Poisson's ratio [-]
Stainless steel	220	0.30
UHMWPE (ISO 5834 -2)	0.69	0.46
Bone cement	2	0.38
Trabecular bone	0.853	0.25

2.7. Numerical analysis results

In the Fig. 2.7. von Mises stress field distribution in the bone-cement interface during one step is depicted. At 20 % of the gait cycle the maximum stress 12.48 MPa was reached in area of the acetabular labrum. In this region the risk of potential damage is expected.

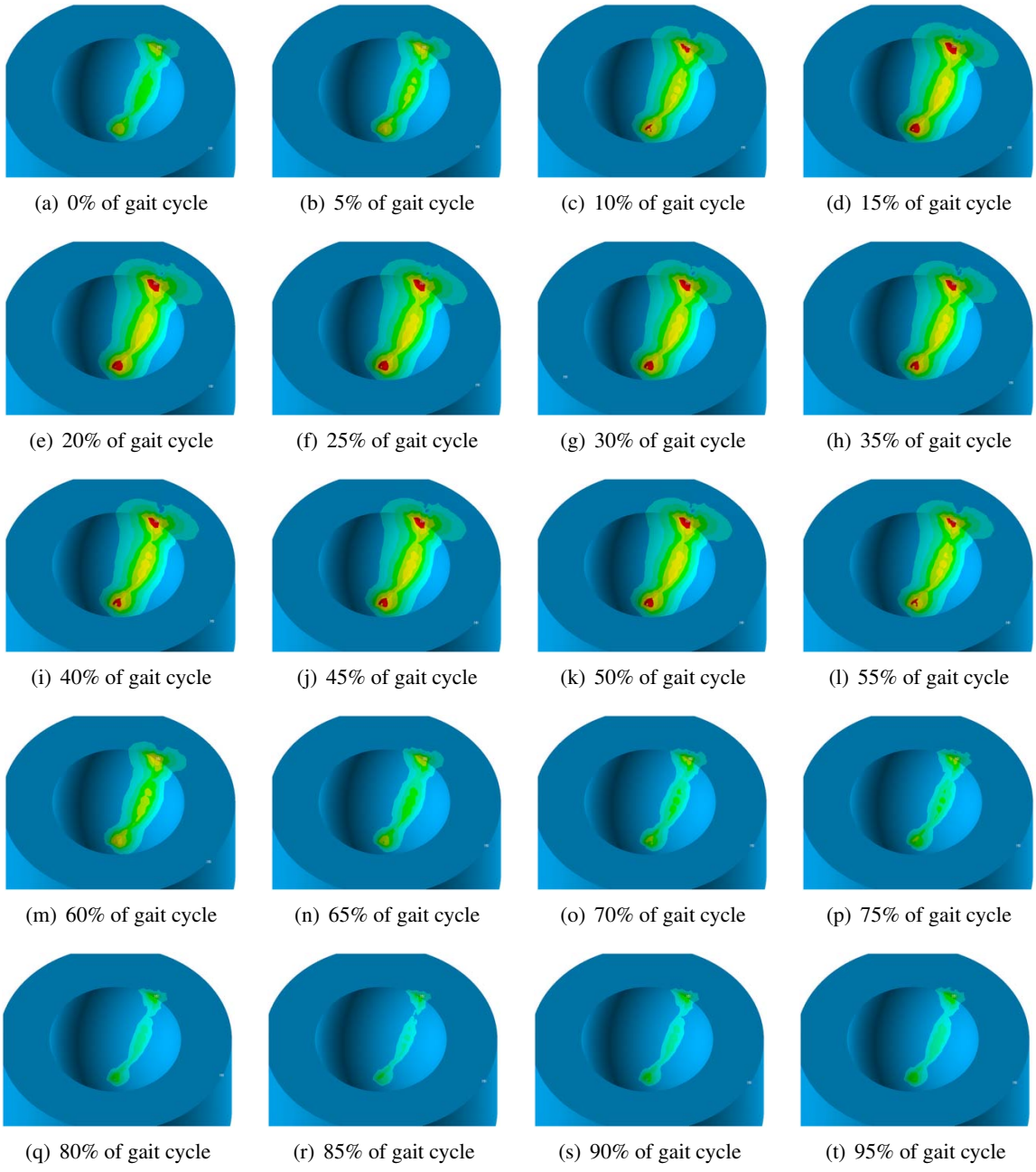

(a) 0% of gait cycle (b) 5% of gait cycle (c) 10% of gait cycle (d) 15% of gait cycle

(e) 20% of gait cycle (f) 25% of gait cycle (g) 30% of gait cycle (h) 35% of gait cycle

(i) 40% of gait cycle (j) 45% of gait cycle (k) 50% of gait cycle (l) 55% of gait cycle

(m) 60% of gait cycle (n) 65% of gait cycle (o) 70% of gait cycle (p) 75% of gait cycle

(q) 80% of gait cycle (r) 85% of gait cycle (s) 90% of gait cycle (t) 95% of gait cycle

Fig. 4: von Mises stress distribution in the bone-cement interface during the normal walking cycle

2.8. Fatigue testing

New hip joint simulator was designed to allow fatigue testing of the sample of pelvic bone with implanted cemented acetabular component. The simulator was designed as an accessory for Instron 1343 (Illinois Tool Works, Inc.). Fatigue tests were carried out using servo-hydraulic loading device. The force-driven loading had a sinusoidal run. The hip contact force of required direction and magnitude was applied to the implant using spherical femoral component head.

According to hip contact forces measurement presented by Bergmann (2001) mean value 1300 N and amplitude 1000 N (the peak value of the contact force corresponds to 260 % of body weight) were chosen to simulate the most unfavorable activity (downstairs walking).

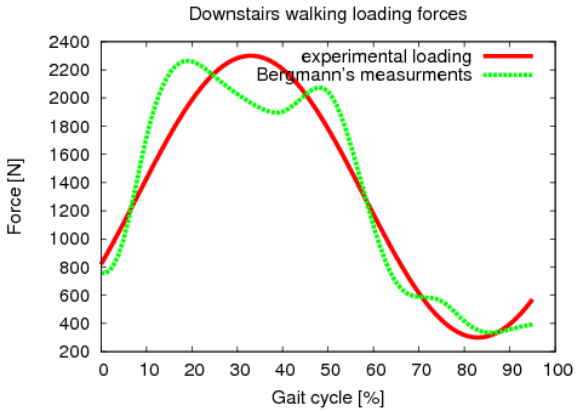

Fig. 5: Comparison of measured hip contact force and experimental loading

The correct position of the bone with the implant and loading force direction was fundamental. Bergmann (2001) measurements and setup of experiments carried out in University of Portsmouth were used. The implanted hemipelvis was mounted onto the loading device for $-8\,^\circ$ on the sagital plane and $-32\,^\circ$ on the transverse plane.

Lewis (2003) tested the effect of loading frequency on the fatigue live of acrylic bone cement. Usually, the experiments are performed with 1 Hz frequency to simulate normal walking. Various types of bone cement specimens were tested by compression test with 1 Hz and 10 Hz frequency. The main conclusion of this study was that the obtained results support the hypothesis that the test frequency (over the range used) does not exert a statistically significant effect on the fatigue live of the cements. According to possibilities of the loading device 4 Hz frequency was chosen for the test.

Fig. 6: The hip simulator

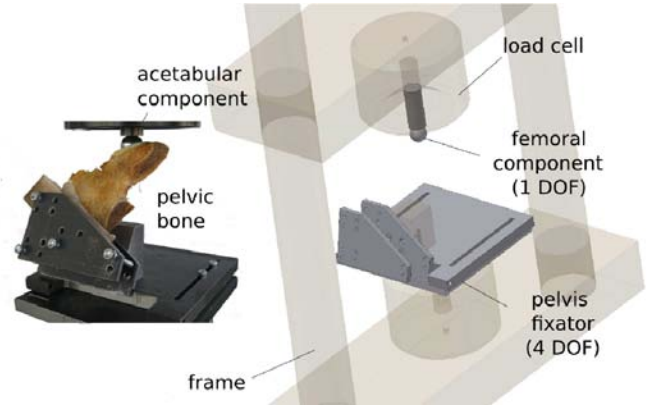

Fig. 7: Design of the hip simulator in detail

The experiment ran for eight hours per a day, that means approximately 115,000 cycles a day. The bone was moistened by saline solution to simulate the physiological conditions during the testing. The temperature in the laboratory was about 25 °C. Between the testing periods the bone was stored in the freezer with temperature $-15\,^\circ$C. Following Grasa (2005) prediction and results of numerical analysis described in section 2.7. the number of loading cycles before imaging with 25 % probability of damage was estimated to 250,000.

2.9. Tomography

High resolution micro-focus X-ray computed tomography (μCT) was used in the investigation of changes in the cement layer cement-bone interface and the actual trabecular bone at the microscopic level. The process of damage accumulation was monitored by repeated scanning. Imaging was performed four times a sample. First the pelvis resected by the dimensions of the corresponding size of the detector with intact acetabulum was scanned. After that the joint replacement was implanted and re-imaged. A quarter of a million load cycles were applied to the pelvis at the hip simulator. After this time some initialization damage of cement could be expected, therefore another scanning has been done. After 300,000 load cycles the pelvis damage was seen with the naked eye, therefore the loading test was completed and final imaging was done.

2.10. Microtomography measurement

To acquire the radiograph of acetabular region microtomography device in detail described in Jakubek (2006) was used. Manipulation with X-ray source, rotation table with specimen and detector was motorized. Stepper motors controlled by Pixelman software plug-in was employed.

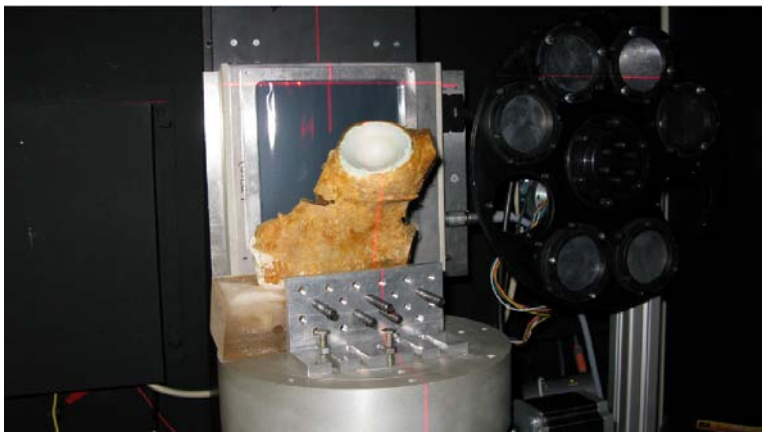

Fig. 8: Pelvis radiogram acquisition using microtomography device

Sequence of 360 projections with $1\,^\circ$ step was acquire using microfocus X-ray source and flat panel detector. Specimen was irradiated using X-ray source L8601-01 (Hamamatsu Photonics K.K.) with emission spot of $5\,\mu\mathrm{m}$. Large area ($120 \times 120\,\mathrm{mm}$)X-ray detector C7942CA-22 (Hamamatsu Photonics K.K.) allowed to obtain image data with resolution up to $2368 \times 2240\,\mathrm{px}$.

To minimize time of scanning the maximal power of the source (voltage $80\,\mathrm{kV}$ and current $125\,\mu\mathrm{A}$) was set. This ratio provide maximal signal to noise ratio in the radiograph. To other improvement of image quality 10 times $0.5\,\mathrm{s}$ acquisition was performed.

2.11. Corrections

Calibration measurements have been held for the noise reduction. Flat field (FF), dark field (DF) and beam hardening (BH) and correction were performed. FF corection (scanning without specimen) reduce the inhomogeneity across the chip. DF correction (scanning with disconnected source) avoids radiation background. BH correction, see Vavrik (2009), was performed to obtain equivalent absorbing characteristic.

2.12. Reconstruction

Tomographic reconstruction is a process which relies on mathematical algorithms to estimate the distribution search space based on 3D projection of 2D data and provides layers (slices) distribution. The sequence of corrected projections were used for object reconstruction. The image reconstruction procedure is based on Filtered Backprojection and Fan beam reconstruction algorithms.

2.13. Specimen visualization

High resolution models based on a sequence of 1100 slices with resolution $2368 \times 2240\,\mathrm{px}$ and $16\,\mathrm{bit}$ color depth were developed to investigate implant degradation during the loading. Projections obtained by μCT imaging were visualized using μCTvis&modeller software, see Vavrik (2011). A visualization of the whole specimen with implanted acetabular component from three different direction before mechanical testing is depicted in Fig. 9. A direct volume rendering technique was used for this purpose.

Fig. 9: Reconstructed acetabulum from different views

3. Results and discussion

A visualization of the damage propagation is shown in 10. There is intacted specimen on the left side. In the middle part the on the pelvis after 250,000 loading cycles crack propagation in trabecular bone structure (marked by the red rectangle) is clearly visible. On the visualization after 300,000 cycles depicted in the right part the crumbled cement particles are identified in green bordered area and cement mantle debonding is marked by the blue rectangle. All these three observed types of damage negatively influence stability of the implant.

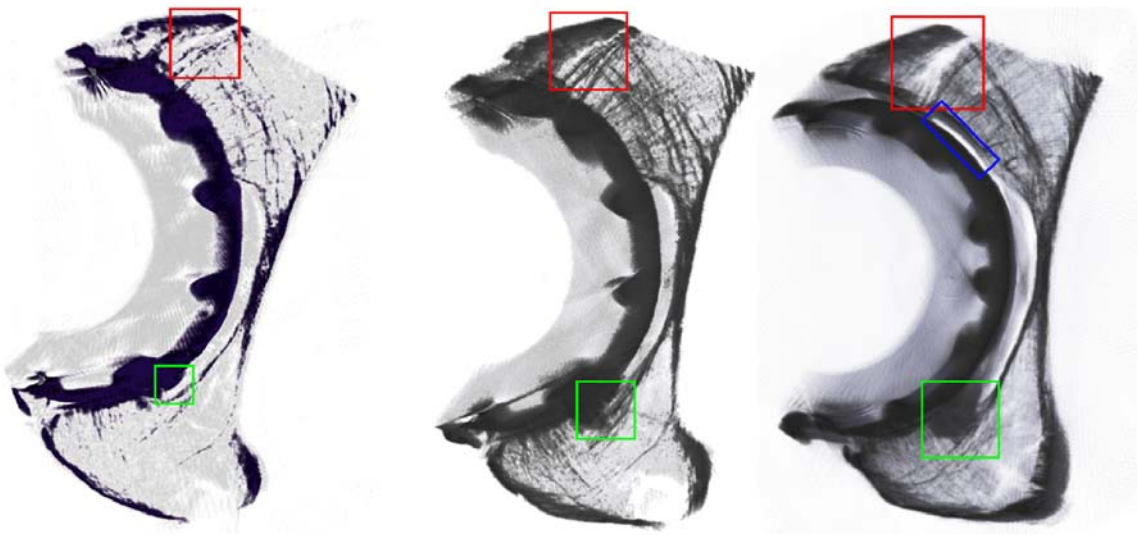

Fig. 10: Damage propagation in the bone structure and cement mantle

In accordance with the results obtained by the FE analysis – stress field with its maximum in region of acetabular labrum – the crack is observable in the same region.

3.1. Model accuracy

The accuracy of the reconstructed model depends on the input data and the reconstruction method. Radiograms could be improved by longer time of radiation. The quality of the reconstructed slices could be improved considerably by increasing the number of projections from 360 to 720 or 1440 in case of 360° tomography. Using cone beam (inclusion of 3D beam divergence effect) results in better data but the required PC-time is not balanced by improvement of model accuracy. Longer radiation and higher number of projections was disapproved because the the X-ray source was loosing its stability with long time of radiation exposure. The other problem with higher number of projections was the hardware limit. The data matrices were exceeding the capacity of the RAM memory of all available computers. Therefore the accuracy of the reconstruction is optimal with respect to the available devices.

4. Conclusions

The aim of the research was to investigate the cemented bone–implant interface behavior (cement layer degradation and bone-cement interface debonding) with an emphasis on the techniques suitable to detect the early defects in the cement layer. The failure of total hip joint replacement was described in this work by the method combining of material testing, numerical simulation, ex vivo experiments and radiological imaging. Mechanical tests were carried out to obtain mechanical properties of trabecular bone and to compare these measurement procedures. Assessed material properties were used in numerical simulations.

The numerical analysis was performed to predict the degradation of acetabular replacement fixation. Detailed three-dimensional finite element model of the acetabular cup and the cement mantle implanted in a small bone block was developed. The analysis of the gait divided in 20 loadsteps ascertained stress field distribution at the bone-cement interface during the gait cycle. The places of maximum value of von Mises stress were in the acetabular labrum for all load steps considered. The place of maximum stress value corresponded well with the place where the initial crack occurred in the experiment. The performed experiments approved accuracy of the numerical model.

To simulate in vivo conditions a polyethylene acetabular cup was implanted into the human pelvic bone using commercial polymethyl methacrylate bone cement. The implanted cup was then loaded in a custom hip simulator to initiate fatigue crack propagation in the bone cement. The pelvic bone was then repetitively scanned in a micro-tomography device. Reconstructed tomography images showed failure processes that occurred in the cement layer during the first 300,000 cycles. Using large area flat panel detector and microfocus X-ray source it is possible to investigate micro-damage propagation in the bone-implant interface.

Presented hybrid experimental–numerical approach allow successful monitoring of cemented hip joint replacement degradation. Particularized three-dimensional finite element model of the acetabular cup and the cement mantle in a small bone block was developed. Numerical analysis was carried out and from stress distribution during gait cycle number of cycles with $25\,\%$ damage probability was estimated. Material properties of the trabecular bone in this model was obtained from mechanical tests. The implanted cup was then loaded in a custom hip simulator to initiate fatigue crack propagation in the bone cement. The crack propagation and debonding was observed using transmission radiography. The replacement degradation was observed at the place predicted by numerical model.

Acknowledgments

The research has been supported by RVO: 68378297, by the Grant Agency of the Czech Republic (grant No. P105/10/2305) and Ministry of Education and Sports (research plan No. MSM6840770040).

References

Bergmann G., Deuretzbacher G., Heller M.O., Graichen F., Rohlmann A., Strauss J. and Duda G.N. (2001), Hip contact forces and gait patterns from routine activities. *J. Biomech.*, Vol 34 No.7, pp 859–871.

Dalstra M., Huiskes R., Odgaard A. and van Erning L. (1993), Mechanical and textural properties of pelvic trabecular bone. *J. Biomech.*, Vol 26, No.4-5, pp 523–535,

Grasa J., Perez M.A., Bea J.A., Garca-Aznar M.J, and Doblare M. (2005), A probabilistic damage model for acrylic cements. Application to the life prediction of cemented hip implants. *Int. J. Fatigue*, Vol 27, No.8, pp 891–904.

Hanson N.A. and Bagi C.M. (2004), Alternative approach to assessment of bone quality using micro-computed tomography. *Bone*, Vol 35, No.1, pp 326–333.

Jakubek J. et al. (2006), Experimental system for high resolution X-ray transmission radiography, *Nucl. Instrum. Meth. A* Vol 563, No.1, pp 278–281.

Jakubek J. (2007), Data processing and image reconstruction methods for pixel detectors, *Nucl. Instrum. Meth. A*, Vol 576, No.1, pp 223–234.

Jirousek O., Zlamal P., Kytyr D., and Kroupa M. (2011), Strain analysis of trabecular bone using time-resolved X-ray microtomography. *Nucl. Instrum. Meth. A*, Vol 633, No.S1, pp S148–S151.

Jirousek O., Jandejsek I. and Vavrik D. (2011), Evaluation of strain field in microstructures using micro-CT and digital volume correlation, *JINST* Vol 6, pp C01039

Lewis G., Janna S. and Carroll M. (2003), Effect of test frequency on the in vitro fatigue life of acrylic bone cement. *Biomaterials*, Vol 24, No.6, pp 1111–1117.

Vavrik D. and Jakubek J. (2009), Radiogram enhancement and linearization using the beam hardening correction method,*Nucl. Instrum. Meth. A* Vol 607, No.1, pp 212–214.

Vavrik D. et al. (2011) Advanced X-ray radiography and tomography in several engineering applications, *Nucl. Instrum. Meth. A* Vol 633, No.S1, pp S152–S155.